WORKING PAPER · SEPTEMBER 2026 · REVISION 10.1 · PART I OF II

Geometry of a Three-Orb Metastructure

A kinematic reconstruction of circulating luminous objects in publicly circulated aircraft footage, with the dynamics it implies

Bryan M. Ingram
Advanced Energy & Frontier Technology
www.bryaningram.com

Part I: Geometry, dynamics and tests

This paper reconstructs the geometry implied by circulating-orb sequences associated with the MH370 video corpus, and works out the forces that geometry would require. It is a model of path and formation, not an authentication of the footage and not a claim that a wormhole was observed.

Abstract

Publicly circulated electro-optical and thermal sequences associated with the so-called MH370 orb corpus show three compact luminous objects moving in coordinated fashion about a wide-body airframe. Treating those objects as real point masses for the purpose of reconstruction — and stating the published counter-evidence on provenance rather than remaining silent on it — this paper writes down the simplest geometry that fits the reported kinematics: a rigid equilateral triad locked at 120° and rotated about the fuselage axis, optionally riding a thin toroidal envelope. With an orbital radius scaled to a 777-class airframe at r = 42 m, the triad has side length $s = r\sqrt{3} \approx 72.7$ m. Circumferential speed is $r\omega$. A weak axial oscillation turns each circular orbit into a flattened helix on the torus, which is the geometric content of the "donut / standing-wave" language used in commentary on the clips. Part I adds the dynamics the kinematics imply: the centripetal requirement and the sign of the coupling it demands, the instability of a passively bound equilateral triad, the spin-up that angular-momentum conservation forces on any collapse, an order-of-magnitude bound on a magnetic binding, the aerodynamic and radiometric budgets, and the energy scale of the "portal" reading. In Part II three candidates are costed against those requirements, a spherical inertial-electrostatic device, a pulsed Z-pinch and a buoyant microwave-sustained plasmoid, the means by which such objects could be steered are examined, the relativity of separated wormhole mouths is reviewed, and a programme of experiments is set out. The model is offered as a measurement frame, not as proof of exotic propulsion.

How the paper is organised. Part I (§§1–8) is the core: what the footage is and is not, the geometry, the dynamics that geometry implies, and the measurements that would confirm or break it. It can be read alone and asks the reader to accept nothing beyond mechanics. Part II (§§9–17) is a companion. It takes the mechanisms that have been proposed for the objects — plasmoids, the Navy filings, three candidate cores, steering by fields, software and intention, and the relativity of separated wormhole mouths — and costs each against the requirements of Part I, keeping what survives. It ends with a programme of work and a closing. Section, equation, figure and reference numbers run continuously through both parts.

Note on this release (Revision 10.1). This paper is the test case of the first in a series of open analyses of theories of everything. The frustration behind the series is that such theories usually stop at the equations: there is rarely a worked example, a current technology the theory speaks to, a derivation a peer can check line by line, or an exercise a student can change a number in and watch. This release therefore pairs the paper with a technical supplement, *The Scaled-Metric Reading*, which adopts five postulates distilled from Dr. Norbert Schwarzer's scaled-metric framework (*Fluid Universe: The Way of Structured Water and its Mathematical Foundations*, Jenny Stanford Publishing, 2026) and re-derives this paper under them; a plain-language guide, *The Seam*; an interactive console in which the formulas can be turned by hand; and a hardware design study published for critique. Dr. Schwarzer reviewed an earlier revision of this paper, and his comments on dimensionality and scale prompted §7.7 and the exercise; he has not reviewed the supplement, the guide or the console, and any error in reducing his framework is the author's. None of it is a claim that the framework is right or that the footage is real. It is an invitation to check the mathematics and to say where it breaks.

PART I

Geometry, dynamics and tests

What the sequences show, the path and formation they imply, the forces that path would require, and the measurements that decide it.

1. Purpose and limits
2. What the sequences appear to show
3. Coordinate frame
4. The path
5. The triangle
6. The torus — the donut envelope
7. Dynamics implied by the kinematics (with 7.7, dimensionality and scale)
8. What would confirm or break the model

1. Purpose and limits

Geometry is prior to interpretation. Before one argues fusion confinement, magnetic reconnection, or topology change, one should be able to say where the objects are, how they move relative to the airframe, and what invariants the formation keeps. The first half of this paper attempts that. The second half asks the next question a physicist would ask: what forces would hold such a path, and what do those forces predict that a drawing does not.

Two limits are binding. First, the clips in circulation have not been authenticated as original sensor records; stereo disparity, platform motion, and compression artifacts remain open, and specific counter-evidence is on the record (§1.1). Second, nothing in a path equation establishes a power source. Field-reversed configuration (FRC) plasmoids and polyhedral cusp confinement are discussed only as the nearest published laboratory geometries that produce self-organized luminous spheres and triangular force-free arrangements — an analogy, not an identification.

The reconstruction is therefore conditional: *if* three compact objects circle a wide-body jet as the sequences depict, *then* the path and the metastructure have the form written below. Falsification is welcome and specified in §8.

1.1 Published counter-evidence

A paper that invites falsification should state what has already been offered. Three items are on the record. First, in August 2023 online analysts matched the terminal flash to a commercial visual-effects element: a shockwave from the Pyromania stock library, first sold on CD-ROM in the 1990s. The initial match covered a single frame and needed distortion to align; proponents call it incomplete, critics call it decisive. Second, in December 2023 the cloud field in the satellite-view clip was matched to stock photographs on textures.com, taken from an airliner near Mt Fuji in 2012 by the artist Jonas De Ro, who has said the images are his. Ashton Forbes disputes the direction of that inference and notes that it does not address the thermal clip. Third, the conventional record is not empty: the Inmarsat handshake sequence defines a final arc in the southern Indian Ocean, and a flaperon recovered on Réunion on 29 July 2015 was identified by French investigators as belonging to 9M-MRO, with further debris recovered on western Indian Ocean shores since [18, 19].

This paper's position follows from its conditional. If the cloud match stands, the satellite-view clip is a composite and the geometry below describes an animation. In that case the dynamics of §7 are the quickest way to show it, because an animator keys positions, not forces, and a keyed path has no reason to conserve angular momentum. If the match fails, the same tests apply to a real volume. Either way the counter-evidence belongs in the first section and not in a footnote.

2. What the sequences appear to show

Across the optical and thermal cuts most often cited in this corpus, three features recur:

- Three compact sources, not one, with apparent angular size well below the airframe.
- Coordinated motion rather than independent drift — the objects keep a mutual spacing while the jet translates.
- A change of mode: an approach or intercept, a circumferential "tune" of order one full rotation, then a tightening or vertical lock immediately before the terminal flash.

Commentary around the clips — notably the analyses gathered by Ashton Forbes and the 4ORBS archive — describes the circumferential phase as a donut or standing-wave wrap about the fuselage, and the locked phase as a triangle whose magnetic pressure then fails inward. Those words already imply a specific manifold. The next sections write it.

Plates I and II are stills pulled from sequences circulating on X in 2026, including the thermal cut in which three compact sources hold station about a wide-body jet (@AshtonForbes, 18 September 2026) and the overhead optical family that shows an airframe, a contrail, and three point sources at once. They are reproduced here as geometric reference, not as authenticated sensor records. HUD-style brackets and corner timestamps visible in several frames are part of the circulating files.

Plate I. Thermal / FLIR stills from the circulating corpus

Public sequences as posted to X, 2026. Used here as geometric reference only.

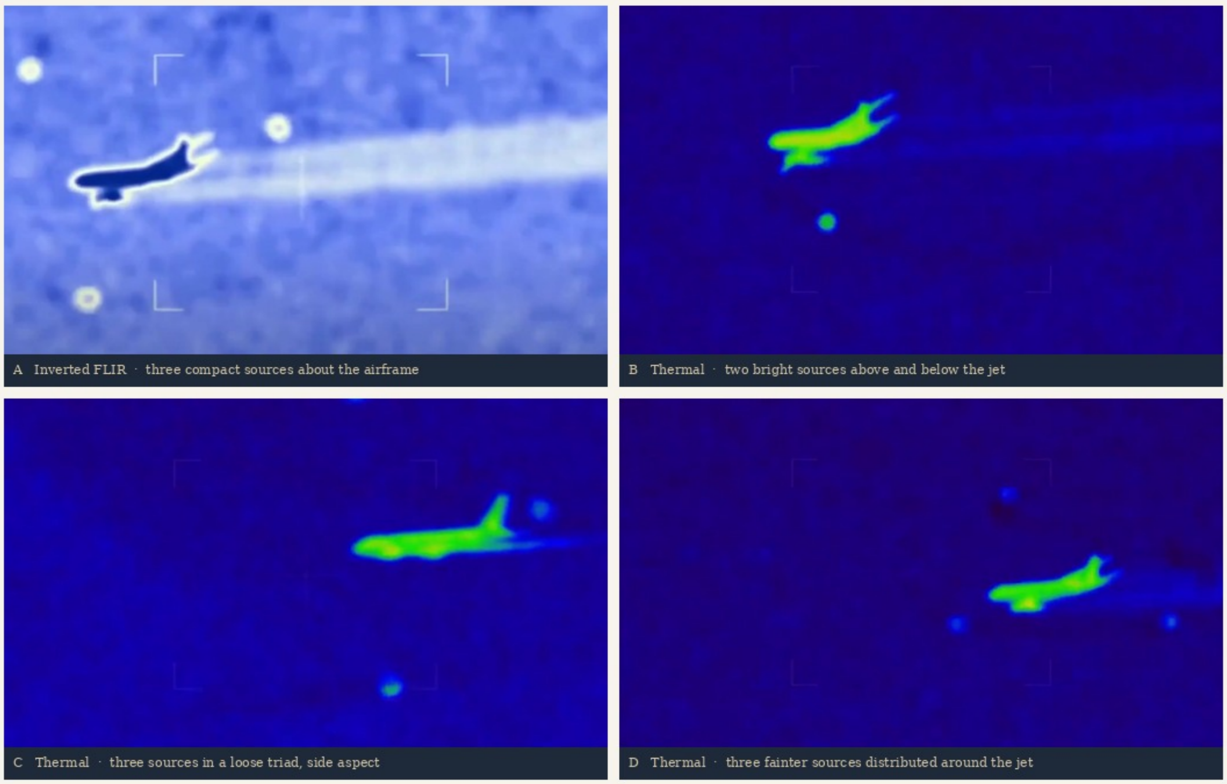

Plate I. Thermal and inverted-FLIR stills. Panel A is the clearest three-source lock in the circulating set. Panels B–D show the same class of compact sources changing station about the airframe — the motion the triad model is written to fit.

Plate II. Overhead optical stills from the circulating corpus

HUD timestamp visible at lower left in several frames of this family.

Plate II. Overhead optical stills from the same corpus family. Panel E is the frame in which an airframe, a contrail, and three compact sources are simultaneously visible. Panel F is the cloud-deck context shot used throughout the optical cuts.

A second circulating military-night-vision file is included because it is the clip most often paired with the MH370 triad in 2025–2026 commentary, and because a senior Ukrainian defence advisor publicly attached the same six-fold morphology to Armed Forces drone collection. On 11 May 2026 the account @airsuperiorx posted an 87-second monochrome sequence labelled "UAP over Ukraine in May of 2025." The HUD in the file reads AIR / TYPHOON. A compact source is tracked against cloud, then resolves on a close pass into a bright core with six radial lobes and a warm axial plume; a conventional airframe and a second compact body appear in other frames (Plate III A–C).

Separately, and on the record, Serhiy "Flash" Beskrestnov — advisor to Ukraine's Ministry of Defence on unmanned systems — published drone video in May 2026 of a rounded object with six pointed cones and a heat plume, recorded by an Unmanned Systems Forces pilot at about 800 m during combat operations. That is the official Ukrainian attachment of this shape to AFU collection. It is not a chain of custody for the TYPHOON-HUD file. A different, earlier AFU corpus is already in the open literature: Mavic 3T thermal records from 2023–2024 of four- and five-sphere formations that are bright in 8–14 µm and dark in the co-bore optical camera. Those spheres travel in a line or a wedge. They do not lock at 120° about an airliner, and they do not show six radial lobes. They belong in the same footnote as the May 2025 star: compact luminous sources under military sensors, different symmetry.

Plate III. Circulating May 2025 night-vision sequence. Stills from the 87-second source file posted by @airsuperiorx.

2.1 The 2026 official releases

Since 8 May 2026 the Department of War has published declassified files on unidentified anomalous phenomena at war.gov/UFO, under the Presidential Unsealing and Reporting System for UAP Encounters (PURSUE). The sixth release, on 18 September 2026, brought the series to several hundred documents, videos and recordings from the Department, AARO, the FBI, the CIA and others. The Department describes the cases as unresolved, meaning that no definitive determination could be made. That is a statement about data, not about origin, and the distinction is old: in a March 1952 talk included in the sixth release, Captain Edward Ruppelt put the residue of good reports from which no conclusion could be drawn at about one in five [29].

Three things in the releases bear on this paper, and one absence. The absence first. The coverage of the six releases consulted for this paper mentions no file that addresses MH370, and none that shows compact sources locked about an airliner; a search of the primary files should confirm that before it is relied on. The releases neither authenticate the clips of Plates I–II nor speak against them; §1.1 stands as written.

What they do supply is official sensor record of the *class*. A 2021 intelligence report on an AC-130J sortie over the Gulf of Oman logs some 25 instances of small dark orbs about 1.2 m across, moving at 250 to 1300 mph in changing formations, and notes that they were cold in the infrared. A 2025 infrared video shows six small spheres over a U.S. military platform at roughly 480 mph, changing direction frequently. Other files show four objects in formation near Iran in 2022 and a larger orb releasing smaller ones. Independent analysts have read several of these videos as small distant infrared features seen with heavy parallax from a moving platform, and that reading has to be held alongside the reported speeds [29].

For the purposes of this paper the consequences are three. The size is useful: a reported diameter of 1.2 m says the $R = 1$ m placeholder of §7 is the right order. The symmetry is not shared: the official formations number two, four, six or a loose swarm, and none is a rigid 120° triad about an airframe, so, like the Ukrainian corpus above, they enlarge the class and leave the manifold where it was. And the thermal sign is a problem for the plasma reading. A 1.2 m sphere at 1300 mph in sea-level air pays, by Equation 12, on the order of 100 MW in drag. An object dissipating that is not cold. Either the speeds are parallax, which is the conventional reading, or the objects do not exchange momentum with the air, which is the strong claim of §7.5 over again. A self-luminous plasmoid is the one reading the word “cold” excludes. The orbs of Plate I, by contrast, are bright in the thermal cut. If both records are taken at face value they are not the same kind of object.

3. Coordinate frame

Place the airframe mid-body at the origin. The flight axis is $+x$ out the nose, $+y$ along the starboard wing, $+z$ toward the upper vertical tail. A Boeing 777-200ER-class geometry supplies the scale: fuselage length ≈ 64 m, wingspan ≈ 61 m, tail height ≈ 18.5 m. The orbital radius used here, $r = 42$ m, is a modeling choice that keeps the triad outside the wingtip circle and consistent with “orbs not on the skin” in the thermal frames. It is not a photogrammetric measurement. Anyone with calibrated plate scale can replace r without touching the form of the equations.

4. The path

The minimal model is three points equally spaced on a circle that lies in a plane perpendicular to the flight axis and is spun about that axis. For orb $i = 0, 1, 2$:

$$\vec{r}_i(t) = (0,\ r\cos(\omega t + 2\pi i/3),\ r\sin(\omega t + 2\pi i/3)),\quad i = 0, 1, 2$$

Equation 1. Parametric path of orb i about the fuselage axis, in the frame of the airframe.

The phase of each orb is $\varphi_i = \omega t + 2\pi i/3$. Differentiating gives the velocity:

$$\vec{v}_i = r\omega\,(0,\ \ -\sin\phi_i,\ \cos\phi_i),\quad |\vec{v}_i| = r\omega,\quad \phi_i = \omega t + 2\pi i/3$$

Equation 2. Velocity of each orb; speed is constant at rω.

A single 360° "receiver tune" before vertical lock is one period $T = 2\pi/\omega$. Path length per orb per turn is $2\pi r \approx 264$ m at the scale chosen here. Because x_i is held at the mid-body station, every orbit lies in a plane normal to the flight axis. That is why a single look-angle can make the objects appear to pass in front of, beside, and behind the jet without a large change in slant range. Equations 1–2 are written in the airframe's frame; the path through the air is a helix and is taken up in §7.5.

5. The triangle

At every instant the three positions are the vertices of an equilateral triangle in the *yz*-plane. Side length, area, and angular momentum about the flight axis (each orb treated as mass *m*) are

$$s = r\sqrt{3},\quad A = \tfrac{3\sqrt{3}}{4}r^2,\quad L_x = 3mr^2\omega$$

Equation 3. Side, area, and axial angular momentum of the rigid triad.

At $r = 42$ m one has $s \approx 72.7$ m and $A \approx 2.29 \times 10^3$ m². The centroid remains on the flight axis for all *t*. That is the geometric meaning of a "metastructure": the triangle is a rigid body in the rotating frame, and any coupling among the three objects — magnetic or otherwise — has L_x as the quantity that can be redistributed if internal spin is torqued into the formation.

If the claimed collapse is real, it is a radial degree of freedom $r(t)$ with $dr/dt < 0$. The triangle remains equilateral while it shrinks until pairwise gaps can no longer support whatever pressure balance is proposed. A collapse trajectory is a one-line extension, $r(t) = r_0 - \alpha t^n$, and should be fitted only against frame-by-frame plate scale. It does not come alone: §7.3 shows that the same L_x fixes what ω must do while *r* falls, and that is the sharpest test in this paper.

6. The torus — the donut envelope

Commentary that the objects "spin around the plane in a donut shape" is a statement about a surface, not a curve. The natural surface is a torus whose major radius is the orbital radius *r* and whose tube radius *a* is the thickness of the luminous sheath or the amplitude of any small radial jitter:

$$x = a\sin v,\quad y = (r + a\cos v)\cos u,\quad z = (r + a\cos v)\sin u$$

Equation 4. Torus of major radius r and tube radius a, axis along x.

A weak axial standing wave — the language of locking vertically, or of a destination on the axis behind the jet — is a small oscillation on x. An earlier draft wrote it as $x_i = A_x \sin \Omega t$ at fixed radius. That curve lies on a cylinder, not on the torus of Equation 4. To ride the torus the axial and radial excursions must move together, with the poloidal angle $v = \Omega t + \delta_i$ and ρ the distance from the flight axis:

$$x_i(t) = a\sin(\Omega t + \delta_i), \quad \rho_i(t) = r + a\cos(\Omega t + \delta_i), \quad a \ll r$$

Equation 5. Axial standing-wave perturbation, written so the path stays on the torus. Each circular orbit becomes a flattened helix.

Three consequences follow. The path closes only if $\Omega/\omega = p/q$ is rational; each orb then traces a (p, q) torus winding — a torus knot when p and q are coprime and both exceed one — and the three orbs together form a three-strand link. A wave that is stationary in the rotating frame, which is what “standing” should mean, requires $\Omega = n\omega$. And the phases matter: with all δ_i equal the triangle breathes along x as a rigid plane, while with $\delta_i = 2\pi i/3$ the plane tilts and the tilt precesses about the flight axis. A side view distinguishes the two.

Figures 1 and 2 render the rigid triad and the perturbed torus at the scale above. The four views in Figure 1 are the same instant. The isometric and along-axis panels make the 120° lock obvious. Top-down collapses the triad toward a line through the mid-body station. The side view shows that every unperturbed path is confined to planes normal to the flight axis.

The May 2025 star in Plate III is a different group. Six lobes at roughly 60° about a single bright core is C_6 symmetry in the plane of the disk, not C_3 symmetry of three separate centers. If those lobes were themselves compact sources on a small circle of radius a, the path would be the same torus equation with $N = 6$ and a much smaller r — a craft-scale hexagram, not an airframe-scale triangle. Nothing in the TYPHOON-HUD file shows three such stars orbiting a jet. The two geometries can live in the same sentence only as members of a class (compact, luminous, multiply-lobed sources under military IR). They are not the same manifold.

Figure 1. Three-orb metastructure about a 777-class airframe · r = 42 m

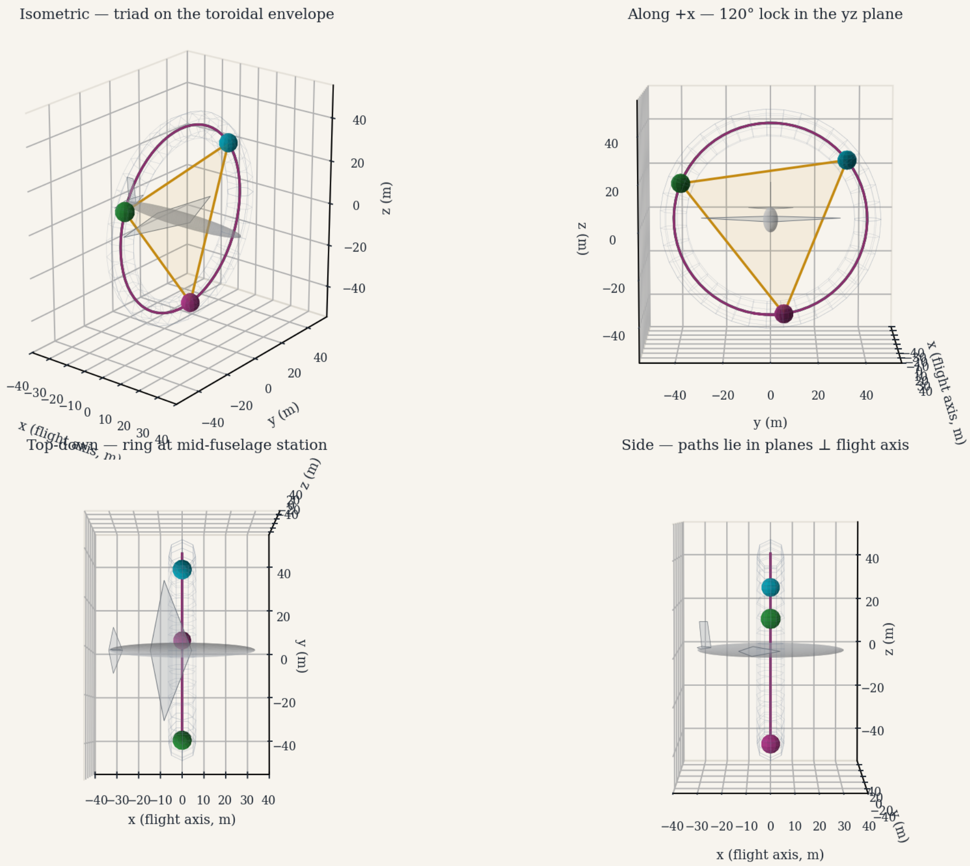

Figure 1. Three-orb metastructure about a 777-class airframe. Orbital radius r = 42 m is a scale choice, not a measurement from the clips.

Figure 2a. yz cross-section of the rigid triad

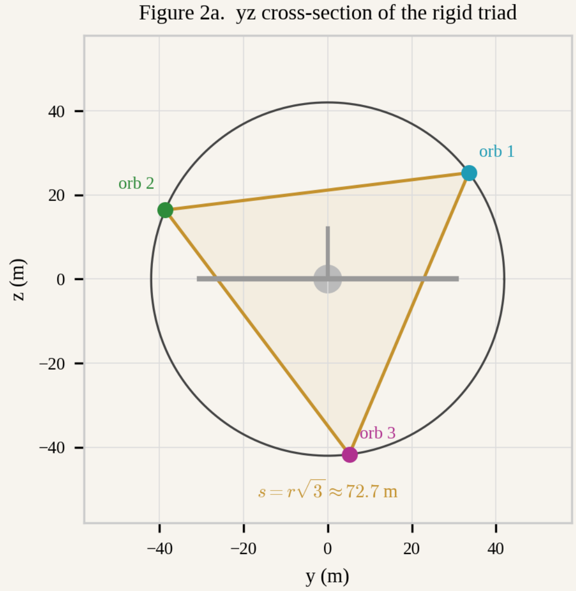

Figure 2b. Torus winding, $\Omega = 3\omega$, $\delta_i = 2\pi i/3$, a = 6 m

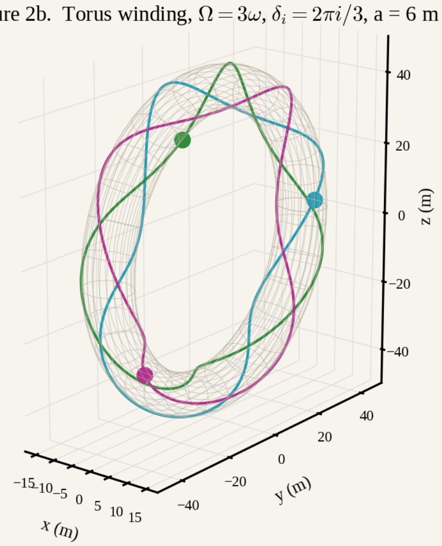

Figure 2. Left: yz cross-section of the rigid 120° triad. Right: the same triad on the torus of Equation 4 with the perturbation of Equation 5 at Ω = 3ω and phases 2πi/3. The tube radius is exaggerated to 6 m so the winding is visible.

7. Dynamics implied by the kinematics

Sections 4–6 say where the objects are. They say nothing about why they stay there. A circle is not a free path: it costs a force, the force has a sign, and the sign and size can be checked against every mechanism proposed for the clips. Numbers in this section assume an orb mass m = 100 kg and radius R = 1 m. Neither is measured. They are placeholders chosen so the scalings can be read, though the 1.2 m diameter logged in the Gulf of Oman file (§2.1) says the radius is of the right order; every result states how it moves with m, R and T.

7.1 The circle costs a force, and the force points inward

Each orb on Equation 1 accelerates toward the flight axis at $r\omega^2$. If the triad is bound by forces between the orbs, the two pair forces on each vertex make 30° with the inward radial, so each pair must *attract* with

$$a_c = r\omega^2 = \frac{4\pi^2 r}{T^2}, \qquad F_{\text{pair}} = \frac{m\,r\omega^2}{\sqrt{3}}$$

Equation 6. Centripetal acceleration of each orb and the attractive pair force that would supply it.

At r = 42 m a four-second rotation is 10.6 g and a two-second rotation is 42 g (Table 1, Figure 3a). That is outside the envelope of any crewed aircraft and inside the envelope of a missile, which is a useful calibration of what is being claimed. More important is the sign. Commentary on the clips, and §9 of this paper, speak of outward magnetic pressure holding the triangle apart. Outward pressure cannot hold a rotating triangle together. Either the net coupling is attractive, or each orb supplies its own inward thrust of $mr\omega^2$ continuously, or the rotation is not mechanical. A reading of the clips has to choose one.

Period T	Orbital speed rω	Centripetal	Speed through air (Mach)	Pair force (100 kg)	Dipole moment M ≥	Surface field (R = 1 m)	Field at fuselage
2 s	132 m/s	42.3 g	283 m/s (0.95)	23.9 kN	10.6×10^8 A·m²	211 T	14 G
4 s	66 m/s	10.6 g	259 m/s (0.87)	6.0 kN	5.3×10^8 A·m²	106 T	7 G
8 s	33 m/s	2.6 g	252 m/s (0.85)	1.5 kN	2.6×10^8 A·m²	53 T	4 G

Table 1. What the circle of Equation 1 costs at r = 42 m, V = 250 m/s, speed of sound 296.5 m/s (ISA, 35,000 ft). Magnetic columns use the most favourable (coaxial) dipole geometry of Equation 10, so they are lower bounds. Moment scales as √m/T; surface field as √m/(T R³).

7.2 A passively bound equilateral triad is unstable

Three bodies at the corners of a rotating equilateral triangle is Lagrange's 1772 solution of the three-body problem. For an inverse-square attraction it is linearly stable only under Routh's condition [20]:

$$\frac{m_1 m_2 + m_2 m_3 + m_3 m_1}{(m_1 + m_2 + m_3)^2} < \frac{1}{27} \qquad (\text{equal masses}: \ \tfrac{1}{3})$$

Equation 7. Routh's stability condition for the Lagrange equilateral configuration. Equal masses fail it by a factor of nine.

Steeper force laws do not help. Under an attractive central force falling as d^{-n} even a two-body circular orbit is unstable for $n \geq 3$, and the dipole–dipole force falls as d^{-4}. Earnshaw's theorem closes the static case. So a triad that holds 120° through a full rotation is not resting in a potential well. It is being actively held, and a control loop leaves a signature. If the binding is modelled as three equal springs of stiffness k, the in-plane modes are one breathing mode and one degenerate doublet [21]:

$$\omega_A^2 = \frac{3k}{m}, \qquad \omega_E^2 = \frac{3k}{2m}, \qquad \omega_A/\omega_E = \sqrt{2}$$

Equation 8. In-plane normal modes of an equal-mass, equal-spring triangle (D3h): breathing mode A and doublet E.

The ratio √2 is independent of *k* and *m*. Rotation splits the doublet through the Coriolis term, and the splitting scales with ω, so it is a second measurement of the spin. The collapse of §5 is the breathing mode going unstable. A spectrum of the residual jitter in angular spacing and radius, taken from stabilised frames, either shows that structure or shows the smooth interpolation of a keyed path.

7.3 Collapse conserves angular momentum

If the triangle tightens without external torque, $L_x = 3mr^2\omega$ is fixed and Equation 3 forces

$$\omega(t) = \omega_0\left(\frac{r_0}{r(t)}\right)^2, \quad v \propto r^{-1}, \quad a_c \propto r^{-3}, \quad K = \frac{L_x^2}{6mr^2}$$

Equation 9. Spin-up, speed, acceleration and kinetic energy of the triad during a torque-free collapse.

Halving the radius quarters the period, multiplies the acceleration by eight and the kinetic energy by four; the attractive coupling must do that work (Figure 3b). This is the sharpest falsifier the clips allow, because it needs no absolute scale: measure ω and the apparent triangle size in the same frames and test whether ωr^2 is constant. A collapse at constant ω means an external torque, a non-mechanical object, or an animation. There is also a hard geometric limit. At the mid-body station the wing occupies the *xy*-plane out to the 30.5 m semi-span, and each orb crosses that plane twice per turn. The triad cannot shrink below $r \approx 30.5$ m, 73 percent of its starting radius, without striking the wing, unless the plane of the triangle first moves off the wing station along *x*. A side view settles which.

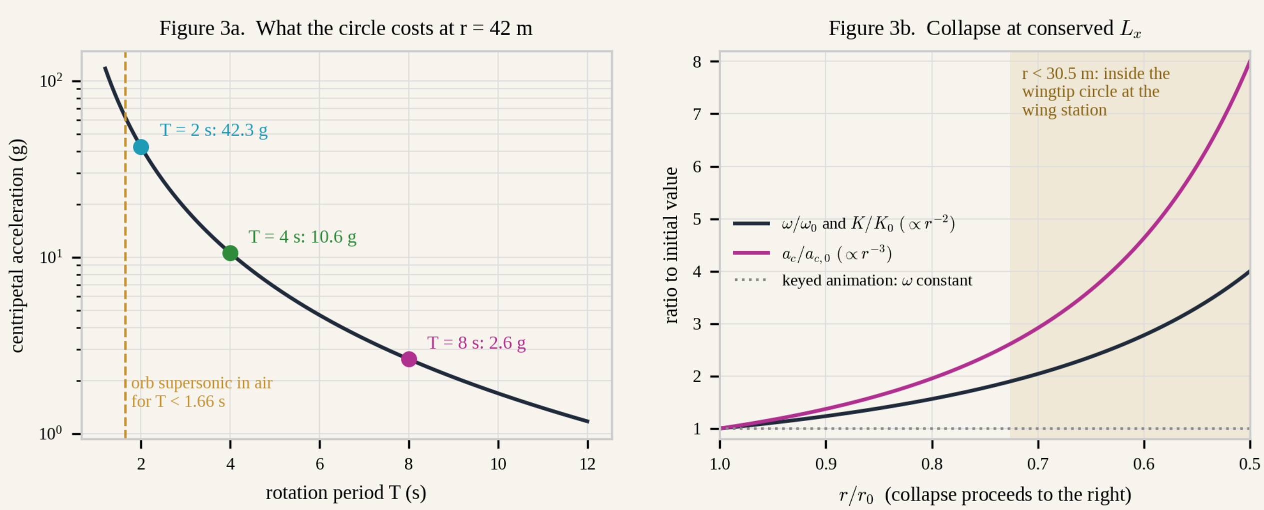

Figure 3. Left: centripetal acceleration on the circle of Equation 1 against rotation period. Right: what Equation 9 requires of a collapse, against the constant-ω path a keyed animation would most naturally follow. The shaded band is forbidden at the wing station.

7.4 A magnetic binding can be bounded

Take the magnetic picture at its word. The strongest attraction two dipoles of moment *M* can exert at separation *s* is the coaxial value, which bounds the moment needed to supply Equation 6 and, through it, the field at the surface of an orb of radius *R* [22]:

$$F_{\max} = \frac{3\mu_0 M^2}{2\pi s^4} \;\Rightarrow\; M \geq \left(\frac{2\pi s^4\, m\, r\omega^2}{3\sqrt{3}\,\mu_0}\right)^{1/2}, \qquad B_{\mathrm{surf}} = \frac{\mu_0 M}{2\pi R^3}$$

Equation 10. Most favourable dipole–dipole attraction, the moment it implies for the triad, and the polar surface field.

For a four-second rotation the moment is 5.3×10^8 A·m² and the surface field about 106 T. The strongest continuous laboratory field is about 45 T, and that magnet fills a room. The same dipoles put roughly 7 G on the fuselage, more than ten times the geomagnetic field, which the aircraft's magnetic heading sensors would register. Two geometric facts make matters worse. Three moments parallel to the flight axis, the arrangement the "outward pressure" language describes, repel one another. And three moments cannot all be pairwise coaxial. A head-to-tail ring in the plane of the triangle attracts, but more weakly than the bound. A magnetic binding is therefore not excluded by geometry, but it is excluded by field strength unless the orbs are far lighter than 100 kg or the rotation far slower than the clips suggest.

7.5 The path through the air

In the air the jet translates at $V \approx 250$ m/s and each orb flies a helix:

$$\vec{R}_i(t) = (Vt,\ r\cos\phi_i,\ r\sin\phi_i), \qquad |\dot{\vec{R}}_i| = \sqrt{V^2 + r^2\omega^2}, \qquad \mathrm{pitch} = VT$$

Equation 11. Path of orb i in the air frame, its speed, and the pitch of the helix.

At $T = 4$ s the pitch is one kilometre, the speed 259 m/s (Mach 0.87), and the velocity is inclined 15° to the flight axis. Below $T \approx 1.66$ s the orbs are supersonic and should drag a shock. The orbit plane sits at mid-body, ahead of where the contrail forms, so the orbs do not cut the contrail itself; an earlier note of mine to that effect was wrong. What they must do, if they are bodies that exchange momentum with the air, is leave three helical wakes of pitch VT wrapped around the contrail at radius r. The jet is drawing a contrail in Plate II E, so the air is cold and moist enough to show one, and a transonic metre-class body in such air leaves a thermal wake and often an aerodynamic condensation trail of its own [25]. No wake means no momentum exchange, which is a strong physical claim, or no body.

7.6 Power: radiated and aerodynamic

Two budgets can be read off a calibrated thermal frame:

$$P_{\mathrm{rad}} = 4\pi R^2\, \varepsilon\sigma T_s^4, \qquad P_{\mathrm{drag}} = \tfrac{1}{2}\rho C_D\, \pi R^2\, |\dot{\vec{R}}|^3$$

Equation 12. Grey-body radiated power of an orb at surface temperature Ts, and the power needed to push it through the air.

For $R = 1$ m a 1000 K surface radiates about 0.7 MW and a 2000 K surface about 11 MW. The sources in Plate I are unresolved, so a radiometric calibration gives the product $\varepsilon R^2 T_s^4$ rather than each factor, but that product is exactly what a power estimate needs. Drag at $C_D \approx 0.5$ and air density 0.38 kg/m³ costs about 5 MW per orb for as long as the formation holds. If the luminous object is a plasma at the ambient 0.24 atm, recombination runs at $\tau \approx 1/(\alpha n_e)$ with α of order 10^{-13} m³/s for molecular ions: 10^{-5} to 10^{-7} s for electron densities of 10^{18} to 10^{20} m^{-3}. Laboratory FRCs live for milliseconds in vacuum. A plasmoid that glows for minutes in the open stratosphere is being fed continuously, at megawatts, from a metre-scale volume, with no visible reaction mass. That is the real size of the claim, and it is better stated than implied.

7.7 Dimensionality and scale

Every result in §§4–7 was derived in a plane, and several of the comparisons in Part II carry a laboratory quantity across many orders of magnitude in size. Norbert Schwarzer, reviewing an earlier revision, warned that neither is bookkeeping: it matters whether a flow is restricted to two dimensions, allowed three, or, in his phrase, “three-plus”, with parameter dependencies entering the equations; and results carry scale dependences that are easy to lose. This subsection records which claims are dimension-sensitive, which cross scales, and one formulation, his, in which both dependences are explicit.

The circle of Equation 1, the pair force of Equation 6, Routh’s condition and the modes of Equation 8 are two-dimensional statements. Out of the plane an equal-spring triangle has three further modes, two rigid tilts and an umbrella, and it is the tilt rather than the breathing mode that the plasmoid analogy of §9 should fear: the fastest-growing instability of a laboratory FRC is the $n = 1$ tilt, invisible in any axisymmetric or planar calculation and found only when the third dimension is admitted [2]. The same is true of the fluid. An orb of metre radius at Mach 0.87 in stratospheric air has a Reynolds number of order 10^7 (about 1.4×10^7 for $R = 1$ m); its wake is three-dimensional and turbulent, and two- and three-dimensional turbulence behave in opposite ways. In two dimensions energy cascades toward large scales and coherent vortices persist; in three dimensions vortex stretching cascades it toward small scales and organised structures are torn apart. A planar model therefore flatters the triad twice. It hides the tilt mode, and it hides the mechanism by which a real atmosphere destroys organised flow. The stability arguments of §7.2 are necessary conditions. They are not sufficient until the tilt is included, and the side view that §7.3 and §11.4 already ask for is the observation that constrains it.

Scale enters in three places, each of which compares a laboratory quantity with an object metres across. Section 11.4 sets a Casimir energy density at 10 nm against the negative energy of a 30 m throat, seventeen orders of magnitude apart in length, and the arithmetic assumes the quantity is the same kind of thing at both scales. Section 13 carries centimetre fireballs fed with kilowatts to metre orbs fed with megawatts, and the scaling is unfavourable: surface losses grow as R^2, the volume to be sustained as R^3, and no published fireball has crossed a decimetre. Section 12 carries a pinch of centimetre radius and a hundred nanoseconds to a sphere of a metre and minutes, and the codes named there include two-dimensional ones; the kink that limits every pinch is a three-dimensional event, and only a three-dimensional result counts for it. Table 2 collects the entries.

Claim	Derived in	Sensitive to	What would settle it
Circle and pair force (Eq. 1, 6)	Plane	Nothing new; exact for a rigid triad	—
Routh condition, spring modes (Eq. 7, 8)	Plane	Out-of-plane tilt and umbrella modes	Side view; tilt precession of Equation 5
Magnetic binding bound (Eq. 10)	Three-dimensional dipoles	None	—
Drag and radiated power (Eq. 12)	Three dimensions, empirical C_D	Re $\approx 10^7$ wake; a 2-D estimate cannot be used	Radiometric calibration of the thermal frames
Plasmoid analogy (§9, §12)	Laboratory, centimetres, vacuum	$n = 1$ tilt and kink (3-D); four to six orders in size and time	Three-dimensional simulation; flicker test of §12.5
Negative-energy comparison (§11.4)	General relativity at 30 m against QED at 10 nm	Whether the comparison is scale-free	Recomputation with a scale factor carried through
Buoyant shell (§13)	Centimetre fireballs	R^2 losses against R^3 volume	Bench test of §16.2

Table 2. Which claims of this paper depend on the dimension in which they were derived or on the scale across which they are compared, and what would settle each. Entries marked — are not at risk.

One formulation makes both dependences explicit rather than implicit, and since it is the source of the warning it is recorded here as a possibility. Schwarzer [39] works from a scaled metric, $G_{\alpha\beta} = F[f]\cdot g_{\alpha\beta}$, inserted into the Einstein–Hilbert action, and shows that the quantum equations then follow from the same variation that gives gravity. Three features bear on this paper. The number of dimensions n appears as a coefficient in the resulting field equations, not as a background assumption: the term nonlinear in the gradient of f grows with n while the curvature terms recede, which is his account of why gravity is weak, and a result derived in a fixed low-dimensional setting does not carry over when parameter dimensions are added — his "3D+". The scale factor $F[f]$ is a choice, of the form $(C_f + f)^{4/(n-2)}$ in the cases he works through, and the physics recovered depends on it, so a quantity such as a vacuum energy density is not scale-free, and a comparison across seventeen orders of magnitude is not guaranteed to be a comparison of like with like. And the action is not taken to be exactly stationary but to sit a parameter off its extremum, what he calls the ever-jittering fulcrum, so that a residual jitter about an equilibrium is expected rather than incidental. He also finds that bounded coherent regions of the scaled field radiate by their nature, with spherical wave solutions of Klein–Gordon type around them.

If that formulation is right, three things in this paper change and one does not. The energy comparison of §11.4 becomes a comparison across scale regimes, and its conclusion, hopeless by seventeen orders of magnitude, would have to be recomputed with the scale factor carried through. This paper does not do that, and does not claim the result would come out favourably; it says only that the present arithmetic assumes what his framework denies. The residual jitter in spacing and radius that §7.2 proposes to measure becomes a quantity with structure of its own rather than a nuisance, though the measurement is the same. And a self-luminous sphere acquires a third reading beside the plasmoid and the fusion core: a coherent domain that radiates because it is bounded, with no reaction inside it at all. The single-band thermal frames cannot separate that from a hot plasma; a spectrum might, since the two need not share a grey-body form. What does not change is the geometry. The circle, the triangle, the torus and the collapse rule are measurements of a path, and they stand or fall on the footage whatever metric underlies it. The paper takes no position on the framework. It records it because it is the only formulation on the table in which the two warnings, dimension and scale, are consequences of the equations rather than cautions attached to them, and because the review that raised them is the review this paper asked for. The author thanks Norbert Schwarzer for the comments that prompted this subsection; any misstatement of his work is the author's.

8. What would confirm or break the model

A model earns its keep by naming the measurement that would kill it. Four tests are geometric:

- **Stereo disparity.** If the circulating files contain two independent views, matching points on airframe, clouds, and each orb must obey one fundamental matrix. A single consistent depth hierarchy — nearby cloud tops shifting more than distant layers, each orb occupying a distinct depth surface — would support a real volume. A uniform horizontal shift would support a duplicated 2-D plate.
- **Angular spacing.** After perspective correction, the three sources should remain near 120° in the plane normal to the fuselage through the locked phase. Systematic drift away from 120° breaks rigidity.
- **Occlusion order.** Front-to-back passages of each orb against the tail and wing must agree with the rotating-triad depth order, not with a flat overlay.
- **Period.** The locked spin should be a single well-defined ω. A changing period that cannot be explained by look-angle, platform motion, or Equation 9 is either a different manifold or an artifact.

Seven more follow from §7, §11.4 and §14 and need no new footage:

- **Spin-up.** Through any tightening, ωr^2 should be constant (Equation 9). Both quantities are image-plane measurements in the same frames, so no absolute scale is required.
- **Mode structure.** Residual jitter of a held formation should show a breathing line and a doublet near $1/\sqrt{2}$ of it, the doublet split in proportion to ω (Equation 8). Smooth interpolation shows neither.
- **Wing clearance.** The triangle cannot pass inside the wingtip circle at the wing station. A side view must show the plane of the triad moving along x before r falls below the semi-span.
- **Wakes.** Three helical trails of pitch VT about the contrail, or a stated reason why a transonic body leaves none.
- **Pointing.** If a fourth source at the destination is taken seriously (§11.4), the locked triad's plane must tilt from the fuselage normal by half the great-circle angle to that destination. An untilted plane names no place on Earth.
- **Shadow and flicker.** If the sources are foci of projected energy rather than bodies (§14.2), each must vanish in the sector where the airframe blocks its beam, and must flicker at the source's pulse rate. Neither is expected of a body or of an overlay.
- **Radiometry.** In-band radiant intensity of each source, converted through Equation 12 to a power, compared with the drag power at the measured speed. The two should be commensurate for any thermal source.

Until those tests are run on original files, the reconstruction remains a hypothesis about shape. That is still useful. A wrong manifold wastes years. A right one tells an experimentalist where to point a sensor.

Part II, published separately, takes up the mechanisms proposed for these objects (§§9–17). Section, equation, figure and reference numbers run continuously through both parts, and the full reference list is given below.

Notes and sources

[1] Public circulating corpus associated with MH370 "Gorgon Stare" / thermal sequences, as compiled and commented by Ashton Forbes (@AshtonForbes) and the 4ORBS evidence library, 2024–2026. Stills in Plates I–II were extracted from clips posted to X, including status/2101012125426839712 (thermal, 18 Sep 2026), status/2101098948119437350 (thermal triad, 19 Sep 2026), status/2083409891105165572 (inverted FLIR), and status/2049183874564121014 (overhead optical family). Reproduced here for commentary and geometric reference. Plate III stills: source file posted by @airsuperiorx, status/2053968963034304788 (11 May 2026, "UAP over Ukraine in May of 2025").

[2] Tuszewski, M. "Field reversed configurations." *Nuclear Fusion* 28, 2033 (1988). Canonical review of compact, self-organized plasmoid equilibria.

[3] Bussard, R. W. "The advent of clean nuclear fusion: superperformance space power and propulsion." 57th International Astronautical Congress (2006). Polyhedral cusp / Polywell architecture.

[4] Pais, S. C. US 10,144,532 B2, "Craft using an inertial mass reduction device" (granted 4 Dec 2018; expired for non-payment). US 10,135,366 B2, electromagnetic field generator. US 10,322,827 B2, high-frequency gravitational wave generator. US 2019/0058105 A1, piezoelectricity-induced room-temperature superconductor (abandoned). US 2019/0295733 A1, plasma compression fusion device (abandoned). All assigned to the U.S. Secretary of the Navy.

[5] Pais, S. C. "The Plasma Compression Fusion Device—Enabling Nuclear Fusion Ignition." *IEEE Transactions on Plasma Science* 47, no. 11 (2019): 5119–5124. doi:10.1109/TPS.2019.2942997.

[6] Pais Effect definition as "controlled motion of electrically charged matter (from solid to plasma) via accelerated spin and/or accelerated vibration under rapid acceleration transients": Pais writings and subsequent interviews; restated in contemporary reporting (The Drive / The War Zone; Big Think, 2021).

[7] NAWCAD public statement: testing of the Pais Effect / HEEMFG from October 2016 to September 2019, approximately $508,000; "the Pais Effect could not be proven." Reported by The War Zone and SpyTalk / The Daily Beast, 2021.

[8] Interviews in which Pais discusses the circulating orb sequences: Ashton Forbes / Dave Rossi, "UFO Disclosure w/ Salvatore Pais" (1 Dec 2024); Forbes, "Salvatore Pais Tells All! MH370 Videos, AI, and ZPE" (25 Jan 2025); Forbes, "Hard Truths /w Sal Pais — Felony Physics Edition" (22 Feb 2026); Jesse Michels conversation as circulated in secondary commentary (singularity remarks; fourth source placed at the destination).

[9] On stereo as a falsifier: a genuine two-view record must admit one fundamental matrix and a layered disparity map. See Hartley & Zisserman, *Multiple View Geometry in Computer Vision*, Cambridge.

[10] Aircraft dimensions: Boeing 777-200ER airport planning data (fuselage length, wingspan, tail height).

[11] Beskrestnov, S. (“Flash”). Public release of Unmanned Systems Forces drone video of a six-cone spherical object with heat plume, combat operations, ~800 m. Reported in Kyiv Post, “Senior Ukraine Official Reports Armed Forces Sighted UFO, Publishes Video,” 12 May 2026.

[12] “Ukrainian Military Observations and Analysis of Aerospace Objects and Phenomena during Defense against the Russian Federation.” Open military/academic compilation (Mavic 3T thermal, 8–14 μm): wedge and in-line formations of four–five spherical objects, 2023–2024; objects bright in IR and dark in co-bore optical on 24 December 2024. See also Main Astronomical Observatory of NAS of Ukraine notes on the 406th Battalion Mavic 3T sequence.

[13] Miley, G. H., Nadler, J., Hochberg, T., Gu, Y., Barnouin, O., Lovberg, J. “Inertial-Electrostatic Confinement: An Approach to Burning Advanced Fuels.” *Fusion Technology* 19, no. 3 (1991): 840–845.

[14] Miley, G. H., Gu, Y., DeMora, J. M., Stubbers, R. A., Hochberg, T. A., Nadler, J. H., Anderl, R. A. “Discharge Characteristics of the Spherical Inertial Electrostatic Confinement (IEC) Device.” *IEEE Transactions on Plasma Science* 25, no. 4 (1997): 733–739. Star-mode microchannels through grid openings.

[15] Miley, G. H., Bromley, B. P., et al. US 6,121,569, “Plasma jet source using an inertial electrostatic confinement discharge plasma” (granted 19 September 2000). Jet-mode extraction from a ported spherical IEC; direct-conversion grids for charged fusion products.

[16] Miley, G. H., and Murali, S. K. *Inertial Electrostatic Confinement (IEC) Fusion: Fundamentals and Applications*. Springer, 2014. Compact IEC as an aneutronic (p–^{11}B) candidate; nested wells. (An earlier note in this draft cited Sved as co-author; the 2014 Springer monograph is Miley and Murali.)

[17] Biographical particulars: University of Illinois NPRE faculty profile; ANS Seaborg Medal citation (advanced-fuel / direct-conversion line); Edward Teller Medal, 1995. Figure 4 left is a laboratory IEC vessel of the Urbana class. Figure 4 right is an artist’s conception of a ported IEC-class sphere in flight configuration (illustration signed Vaughan; hull marked Inertial Dynamics), reproduced here as a topology reference, not as a program document.

[18] Counter-evidence on the clips: “The MH370 Teleport Hoax,” *Skeptical Inquirer*, February 2024; community compilation of the August 2023 Pyromania “Shockwave” element comparison and the December 2023 textures.com cloud-photograph match (photographs by Jonas De Ro, 2012), with Forbes’s published rebuttals. Readers should consult both sides’ primary posts; this paper takes the matches as open challenges the footage must answer, not as settled by citation.

[19] Conventional record: Ashton, C., Shuster Bruce, A., Colledge, G., Dickinson, M. “The Search for MH370.” *Journal of Navigation* 68 (2015): 1–22 (Inmarsat burst-timing and burst-frequency analysis). Australian Transport Safety Bureau, *The Operational Search for MH370* (2017). Flaperon recovered on Réunion 29 July 2015 and attributed to 9M-MRO by French judicial authorities, September 2015.

[20] Routh, E. J. “On Laplace’s three particles, with a supplement on the stability of steady motion.” *Proc. London Math. Soc.* 6 (1875): 86–97. Modern treatment in Danby, *Fundamentals of Celestial Mechanics*. Stability of circular orbits under power-law forces: Goldstein, *Classical Mechanics*, ch. 3.

[21] Normal modes of the equilateral X_3 system: Herzberg, G. *Infrared and Raman Spectra of Polyatomic Molecules* (1945). The mode frequencies and the √2 ratio in Equation 8 were also checked numerically for this paper.

[22] Dipole–dipole force and dipole fields: Jackson, J. D. *Classical Electrodynamics*, 3rd ed., ch. 5. Continuous-field record of about 45 T: National High Magnetic Field Laboratory hybrid magnet.

[23] Morris, M. S., and Thorne, K. S. “Wormholes in spacetime and their use for interstellar travel.” *Am. J. Phys.* 56 (1988): 395–412. Visser, M. *Lorentzian Wormholes* (AIP, 1995). Ford, L. H., and Roman, T. A. “Averaged energy conditions and quantum inequalities.” *Phys. Rev. D* 51 (1995): 4277.

[24] Schwinger, J. “On gauge invariance and vacuum polarization.” *Phys. Rev.* 82 (1951): 664. Vacuum magnetic birefringence searches: PVLAS collaboration.

[25] Atmosphere at 35,000 ft (ISA): density 0.380 kg/m³, pressure 23.8 kPa, speed of sound 296.5 m/s. All numerical values in §7, §10.4 and §11.4 were computed from the stated formulas with m = 100 kg and R = 1 m as placeholders, not measurements.

[26] Lockheed Martin Compact Fusion Reactor: Chase, C., Solve for X presentation, 7 February 2013. Norris, G. “Skunk Works Reveals Compact Fusion Reactor Details.” *Aviation Week & Space Technology*, 15 October 2014. McGuire, T. J. US 9,934,876 B2 and US 9,947,420 B2, “Magnetic field plasma confinement for compact fusion power”; McGuire, US–Japan Compact Torus Workshop presentation (2016), T4/T4B parameters. T5 statement by J. Babione reported by The War Zone, July 2019. Trimble, S. “Skunk Works Halted Nuclear Fusion Effort Before 2021.” *Aviation Week*, 30 August 2023.

[27] TAE Technologies FRC program: Binderbauer, M. W., et al. “A high performance field-reversed configuration.” *Phys. Plasmas* 22, 056110 (2015). Limits on thermal p–^{11}B: Rider, T. H. “Fundamental limitations on plasma fusion systems not in thermodynamic equilibrium.” *Phys. Plasmas* 4, 1039 (1997).

[28] Casimir, H. B. G. *Proc. K. Ned. Akad. Wet.* 51, 793 (1948). Wilson, C. M., et al. “Observation of the dynamical Casimir effect in a superconducting circuit.” *Nature* 479, 376 (2011). Nobel Prize in Physics 2025 (Clarke, Devoret, Martinis): macroscopic quantum tunnelling and energy quantisation in an electric circuit.

[29] U.S. Department of War, PURSUE (Presidential Unsealing and Reporting System for UAP Encounters), war.gov/UFO: six releases, 8 May, 22 May, 12 June, 10 July, 7 August and 18 September 2026; press release "Department of War Publishes Sixth Release of Unidentified Anomalous Phenomena Files," 18 September 2026. Cases cited here as summarised in EarthSky's coverage of the fifth and sixth releases (Gulf of Oman AC-130J report, 8 September 2021; six-sphere infrared video, 2025; Ruppelt talk, 26 March 1952; AAWSAP Defense Intelligence Reference Documents). Independent video analysis: Metabunk, "War.gov/UFO — Department of War Releases UAP Files," 2026. The primary files should be consulted before any figure here is relied on.

[30] Defense Intelligence Agency, Defense Intelligence Reference Documents produced under the Advanced Aerospace Weapon System Applications program and published by the Department of War as DOW-UAP-D139 and DOW-UAP-D153 (PURSUE sixth release, 18 September 2026): "Traversable Wormholes, Stargates, and Negative Energy," DIA-08-1004-004, 6 April 2010 (Equation 8, Casimir plate spacing; Equation 9 and Table 2, negative equivalent mass; §II-C, appearance of a throat; §III-B, laboratory sources); "Quantum Tomography of Negative Energy States in the Vacuum," DIA-08-1102-007, 11 January 2011 (balanced homodyne detection of sub-vacuum fluctuations). Author names are redacted in the released copies.

[31] Einstein, A., and Rosen, N. "The particle problem in the general theory of relativity." *Phys. Rev.* 48 (1935): 73. Gao, P., Jafferis, D. L., and Wall, A. C. "Traversable wormholes via a double trace deformation." *JHEP* 12 (2017): 151. Maldacena, J., Milekhin, A., and Popov, F. "Traversable wormholes in four dimensions." arXiv:1807.04726 (2018). Jafferis, D., et al. "Traversable wormhole dynamics on a quantum processor." *Nature* 612 (2022): 51–55; the interpretation of that experiment is debated. Squeezed light in gravitational-wave detectors: Tse, M., et al. *Phys. Rev. Lett.* 123, 231107 (2019). First detection: Abbott, B. P., et al. *Phys. Rev. Lett.* 116, 061102 (2016).

[32] Staged Z-pinch. Publications as listed by the developer: Rahman, H. U., Wessel, F. J., and Rostoker, N., *Phys. Rev. Lett.* 74, 714 (1995); Rahman et al., *Phys. Plasmas* 11, 5595 (2004); *J. Plasma Phys.* 75, 749 (2009); *Astrophys. Space Sci.* 323, 51 (2009); *Phys. Plasmas* 19, 122701 (2012); *Phys. Plasmas* 26, 052706 (2019); Conti et al., *Phys. Plasmas* 27, 012702 (2020); Ruskov et al., *Phys. Plasmas* 27, 042709 (2020) and 28, 112701 (2021). A 1997 entry is given in the source as "Physics of Plasmas 58, 367", which does not match that journal's volume numbering and should be checked. Patent: US 9,839,111 B2, "Staged Z-pinch for the production of high-flux neutrons and net energy." Facilities, yields, roadmap, science team and advisory board: MIFTI Fusion company presentation, September 2025, cited with the company's permission; financing terms in that document are not reproduced here. Independent corroboration of the Zebra result: APS Division of Plasma Physics 2017, UP11.125; Double-EAGLE experiment: LLNL-JRNL-2021661; company background: Lyncean Group summary (2021); ARPA-E ALPHA award, 2015.

[33] Knuth, K. H., Powell, R. M., and Reali, P. A. "Estimating Flight Characteristics of Anomalous Unidentified Aerial Vehicles." *Entropy* 21 (2019): 939. Nimitz 2004 witness and radar accounts as summarised there.

[34] Bobrick, A., and Martire, G. "Introducing physical warp drives." *Class. Quantum Grav.* 38 (2021): 105009. Fuchs, J., Helmerich, C., Bobrick, A., Sellers, L., Melcher, B., and Martire, G. "Constant velocity physical warp drive solution." *Class. Quantum Grav.* 41 (2024): 095013.

[35] Morris, M. S., Thorne, K. S., and Yurtsever, U. "Wormholes, time machines, and the weak energy condition." *Phys. Rev. Lett.* 61 (1988): 1446. Friedman, J., et al. "Cauchy problem in spacetimes with closed timelike curves." *Phys. Rev. D* 42 (1990): 1915. Echeverria, F., Klinkhammer, G., and Thorne, K. S. *Phys. Rev. D* 44 (1991): 1077. Kim, S.-W., and Thorne, K. S. *Phys. Rev. D* 43 (1991): 3929. Hawking, S. W. "Chronology protection conjecture." *Phys. Rev. D* 46 (1992): 603.

[36] "KSM Rocket Booster / Engine — FRC-EVO Maximum Efficiency," unattributed graphic circulated on X, 2026; described here, not reproduced. LINUS: Turchi, P. J., et al., Naval Research Laboratory imploding-liner program, 1970s. Dense plasma focus with p–^{11}B: Lerner, E. J., et al., *Phys. Plasmas* 19, 032704 (2012). Shoulders, K. R., *EV: A Tale of Discovery* (1987), for the original exotic-vacuum-object claims. Neutron-producing side reactions in p–^{11}B: see Rider [27].

[37] "Plasma Buoyancy and Trans-Domain Flight: A Classroom Discussion," April 2026, circulated under the series title "McCasland Archive Technical Series"; author not stated, and no connection to any named individual is asserted here. Atmospheric fireballs: Ohtsuki, Y. H., and Ofuruton, H. "Plasma fireballs formed by microwave interference in air." *Nature* 350 (1991): 139. Dikhtyar, V., and Jerby, E. "Fireball ejection from a molten hot spot by localized microwaves." *Phys. Rev. Lett.* 96, 045002 (2006). Added mass and the 2 g limit: Batchelor, G. K. *An Introduction to Fluid Dynamics*, §6.8. Oxygen absorption at 60 GHz: ITU-R Recommendation P.676. TOPAZ: flown on Kosmos 1818 and 1867, 1987. Haisch, B., Rueda, A., and Puthoff, H. E. *Phys. Rev. A* 49 (1994): 678. Energy deposition for drag reduction: Knight, D. *J. Propulsion and Power* 24 (2008): 1153. Gas cavities and drag under water: Ceccio, S. L. *Annu. Rev. Fluid Mech.* 42 (2010): 183.

[38] Steering. RF thruster concept: "Dual-Frequency RF Plasma Thruster with Solid Hydrocarbon Propellant," unpublished student concept paper, Kevin T. Crofton Department of Aerospace and Ocean Engineering, Virginia Tech, summer 2026 (author not named in the copy seen); baseline data as cited there from Lee et al., *Scientific Reports* (2025). Magnetic-nozzle thrust steering: Imai, R., and Takahashi, K. *Appl. Phys. Lett.* 118, 264102 (2021). Ion-wind flight: Xu, H., et al. *Nature* 563 (2018): 532. Laser-induced plasma decoys: US 11,359,892 B2 (U.S. Navy, 2022). Aerial plasma images: Ochiai, Y., et al. *ACM Trans. Graphics* 35, no. 2 (2016): 17. Learned plasma control: Degrave, J., et al. *Nature* 602 (2022): 414. Brain–computer interfaces: Hochberg, L. R., et al. *Nature* 485 (2012): 372; LaFleur, K., et al. *J. Neural Eng.* 10, 046003 (2013); Willett, F. R., et al. *Nature* 593 (2021): 249. Intention and random generators: Jahn, R., et al. *J. Scientific Exploration* 14 (2000): 499 (consortium replication); Bösch, H., Steinkamp, F., and Boller, E. *Psychological Bulletin* 132 (2006): 497. Orchestrated objective reduction: Hameroff, S., and Penrose, R. *Physics of Life Reviews* 11 (2014): 39; Tegmark, M. *Phys.*

Rev. E 61 (2000): 4194. The author's earlier protocol: Ingram, B., "Efficient Traversable Wormhole Portal System," unpublished, January 2026.

[39] Schwarzer, N. *Fluid Universe: The Way of Structured Water and its Mathematical Foundations*. Jenny Stanford Publishing, 2026. ISBN 9789815352153. Scaled metric $G_{\alpha\beta} = F[f]\cdot g_{\alpha\beta}$ within the Einstein–Hilbert action; explicit dependence of the field equations on the dimension number; non-extremal ("ever-jittering fulcrum") variational principle; radiating coherent domains. Comments on dimensionality and scale: private communication to the author, September 2026. Earlier exposition: Schwarzer, N. *The Theory of Everything: Quantum and Relativity is Everywhere – A Fermat Universe*. Jenny Stanford Publishing, 2020. FRC tilt instability: see Tuszewski [2].

Bryan M. Ingram works at the intersection of aneutronic energy, water technology, and frontier measurement. Correspondence: bryaningram.com. Views in this working paper are the author's and do not represent any laboratory, agency, or venture named on that site.